Supporting Information

Wide-Temperature Flexible Polyurethane Network Reinforced PVDF-HFP Electrolytes for Solid-State Lithium Metal Batteries Operated Under Extreme Conditions

*Kaidong Zhang, Jing Yang, Kangshuai Zhu, Tongle Xu and Qinmin Pan**

State Key Laboratory of Space Power-Sources, MOE Engineering Research Center for Electrochemical Energy Storage and Carbon Neutrality in Cold Regions, School of Chemistry and Chemical Engineering, Harbin Institute of Technology, Harbin 150001, China

*Corresponding author.

E-mail: panqm@hit.edu.cn

Experimental section

Chemicals

Polypropylene carbonate diol (PPCD, Macklin), isophorone diisocyanate (IPDI, Aladdin), 1,1,1-tris(hydroxymethyl)propane (TMP, Aladdin), ditin butyl dilaurate (DBTDL, Macklin), acetonitrile (ACN, Aladdin), 1-methyl-2-pyrrolidinone (NMP, Aladdin), polyvinylidene fluoride-hexafluoropropylene (PVDF-HFP, Macklin) and lithium bis (trifluoromethylsulfonyl) imide (LiTFSI, Aladdin) were used as received.

Synthesis of cross-linked PU

Two-step method involving prepolymerization and chain extension was utilized to yield polyurethane (PU). First, 1 g PPCD, 0.445 g IPDI with 0.01 g DBTDL were dissolved in 10 mL ACN and then heated at 80℃ for 5 hours to yield the PU prepolymer in argon atmosphere. Subsequently, crosslinking agent TMP was added to the prepolymer, and the mixture was heated at 80℃ for an additional 2 hours to yield cross-linked PU.

Synthesis of SPEs

PVDF-HFP and LiTFSI were stirred in 10 mL of NMP at 80 °C until a clear solution was obtained. This solution was mixed with a PU solution in ACN in a specific proportion, then heated at 80 °C under stirring for 2 hours. The resulting mixture was coated onto a polyethylene terephthalate film at room temperature for 12 hours. Subsequently, the coated film was placed in an oven at 60℃ for 12 hours. Finally, the sample was dried in a vacuum oven at 80℃ for 24 hours to yield the SPE film. To identify the optimal formulation, three electrolytes with varying PVDF-HFP to PU

mass ratios were prepared and labeled 3PH-PU-SPE, PH-PU-SPE, and PH-3PU-SPE. Their respective mass ratios were 3:1, 1:1, and 1:3. A similar procedure was employed to prepare the PH-SPE.

Characterizations

Chemical structure of PU was identified by Fourier transform infrared spectroscopy (FT-IR, Alpha Platinum ATR, Bruker). Microscopic morphology of the electrolyte membrane was observed using a field emission scanning electron microscope (FE-SEM, S-4800, Hitachi). X-ray diffraction (XRD) analysis was conducted on a Rigaku SmartLab3. Thermogravimetric analysis (TGA) was performed using a TG/DTA7300 thermogravimetric/differential analyzer with a heating rate of 10°C/min. Differential scanning calorimetry (DSC) was performed on a Netzsch DSC 200 F3 with a heating rate of 10°C/min. X-ray photoelectron spectroscopy (XPS) was performed on an Axis Ultra DLD Kratos AXIS SUPRA. The tensile and puncture stress-strain curves of the strip were tested by an INSTRON 5565 testing system. Electrochemical impedance spectroscopy (EIS) and cyclic voltammetry (CV) tests were performed on an electrochemical workstation (CHI650D).

Ionic conductivity measurements

Ionic conductivity of electrolytes was determined by electrochemical impedance spectroscopy (EIS) on the electrochemical station CHI650D in the frequency range of 10^6–0.1 Hz with an AC amplitude of 5 mV in the temperature range from 30°C to 80°C. The ionic conductivity was calculated by the following equation

$$\sigma = \frac{L}{R \times A}$$

where R, L and A are the bulk resistance, thickness, surface area of electrolytes, respectively.

The activation energies of SPE were fitted by the Arrhenius equation

$$\sigma = Aexp(-\frac{E_a}{RT})$$

where A is the pre-exponential factor, E_a is the activation energy, R is the molar gas constant, T is the absolute temperature.

Li-ion transference number measurements

The Li-ion transference number (t_{Li+}) was obtained by a chronoamperometry test with a voltage amplitude of 10 mV and EIS tests taken before and after DC polarization on symmetric Li|SPEs|Li cells. The value of t_{Li+} can be calculated according to equation

$$t_{Li+} = \frac{I_{ss}(\Delta V - I_0 R_0)}{I_0(\Delta V - I_{SS} R_{SS})}$$

where I_0 and I_{ss} are the initial and steady-state DC current, R_0 and R_{ss} are the initial and steady-state interfacial resistances, and ΔV is the applied potential, respectively.

Electrochemical stability window measurements

Electrochemical stability window of SPEs was estimated by linear sweep voltammetry (LSV) test on Li|SPEs|SS cells at a scan rate of 0.1 mV/s from open-circuit voltage (OCV) to 6.0 V at room temperature.

Li-ion diffusion coefficient measurements

The Li|SPEs|Li cells are polarized at 5 mV before the potential is interrupted. Once the potential was interrupted, the cell was kept at OCV until a stable state was achieved. Later, the profiles are plotted as the natural logarithm of potential (V) versus time (t). The D_{Li+} values were calculated from the slope of the plots using the following equation

$$Slope = \frac{\pi^2 \times D_{Li^+}}{L^2}$$

where L is the thickness of electrolytes.

Preparation of cathodes

The cathode slurry was prepared by dispersing $LiFePO_4$ or NCM811, SPE, acetylene black and PVDF (mass ratio = 6: 2: 1: 1) in NMP under stirring for 8 h. The slurry was coated onto an Al foil and then dried at 80°C for 24 h under vacuum. The resulting foil was punched into circular disks with a diameter of 14 mm. The mass loading of active material was 1.5-2.0 mg/cm^2.

Assembly and test of SSBs

Solid-state batteries were assembled with LFP or NCM811 cathodes, lithium foils and SPE in an argon-filled glove box (H_2O < 0.1 ppm, O_2 < 0.1 ppm, mikrouna). Similarly, a pouch battery was assembled by using a LFP electrode (28 mm × 29 mm), Li foil (30 mm × 30 mm), and 3PH-PU-SPE (35 mm × 35 mm) were packed in an aluminum-plastic film pouch. Solid-state Li||LiFePO4 batteries were tested at a voltage range of 2.5−3.8 V, while solid-state Li|NCM811 batteries operated in a voltage range of 2.8−4.3 V. All the solid-state batteries were evaluated using a Neware battery tester (China).

Symmetric Li|SPEs|Li cells were tested at a current density of 0.1 mA/cm^2 and a capacity of 0.1 mAh/cm^2 at room temperature. The Li dendrite suppression capability of the SPEs was evaluated through critical current density (CCD) testing from 0.1 to 1 mA/cm^2.

Theoretical calculation

Quantum chemical calculations were carried out via Gaussian 16W using density functional theory (DFT) with the B3LYP functional and 6-311G(d,p) basis set. The highest occupied molecular orbital (HOMO) and lowest unoccupied molecular orbital (LUMO) energies were obtained. The binding energy (ΔE_b) was calculated by the equation

$$\Delta E_b = \Delta E_{total\,(a-b)} - \Delta E_{total(a)} - \Delta E_{total(b)}$$

where E_{total} is the energy calculated by the DFT of the corresponding systems.

Molecular dynamics (MD) simulations were performed using the Materials Studio 2023 software, particularly employing its Forcite module to characterize and quantify the intermolecular interaction forces within the system of interest. A periodic boundary condition (PBC) and cutoff energy of 400 eV were applied to the box. After establishing the box with optimized configuration, an anneal procedure from 300 to 400 K in 1.0 atm was carried out for 2 ns to reach equilibrium state with minimum local energy, based on conjugate gradient method. Afterwards, a dynamic procedure was also conducted with NPT ensemble for 1 ns to relax, and MD simulation was then continued with additional simulation time of 2 ns (the time step was set to 1 fs) to transform from NVT ensemble to NVE to collect molecular/ion coupling data. To be noticed, all the temperature is controlled with Nose thermostat. Radial Distribution Function (RDF) of Li^+ and O atom of $TFSI^-$ were also calculated employing MD simulation. Mean squared displacement (MSD) was recorded every time step to acquire Li^+ diffusion dynamics at different locations of the composite electrolytes.

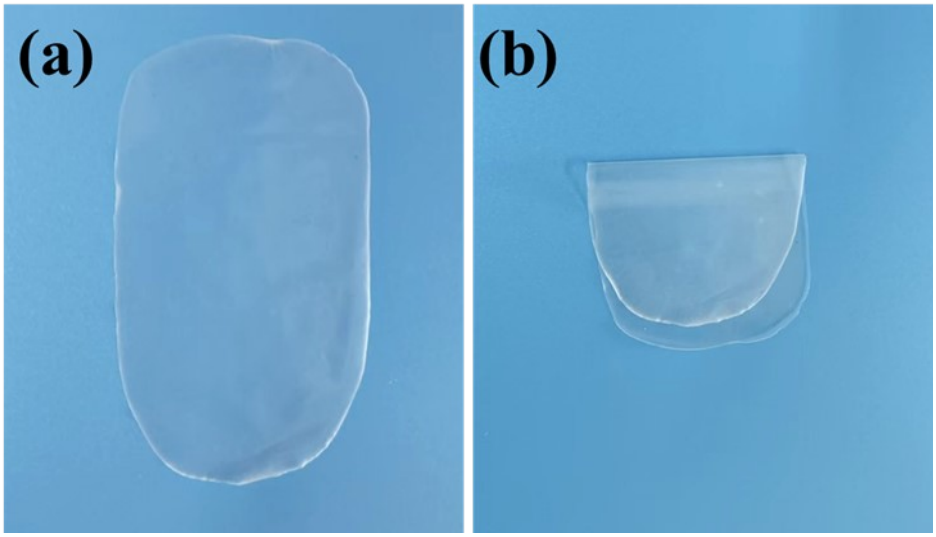

Fig. S1. Digital photographs of (a) 3PH-PU-SPE film and (b) its folded state.

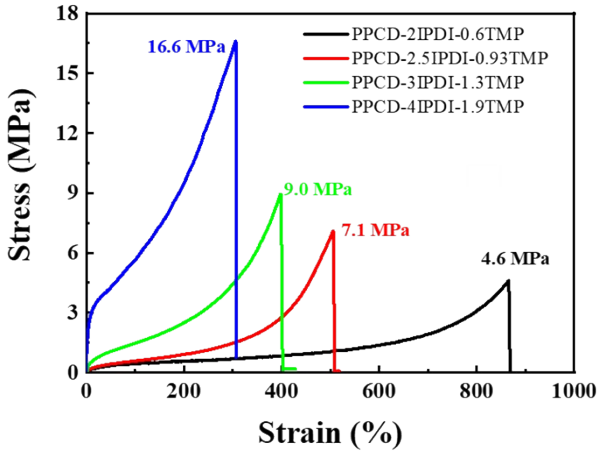

Fig. S2. Stress-strain curves of the PU films with various crosslinker ratios.

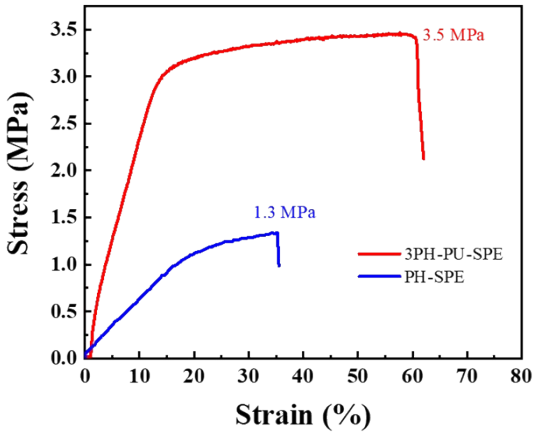

Fig. S3. Stress-strain curves of 3PH-PU-SPE and PH-SPE films.

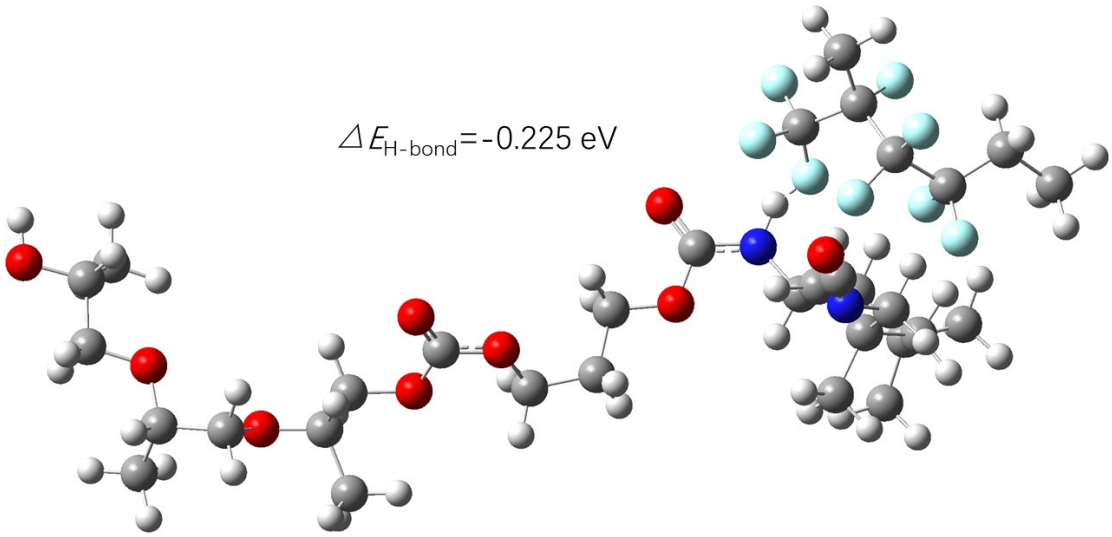

Fig. S4. DFT calculation of H-bond binding energies between PVDF-HFP with PU.

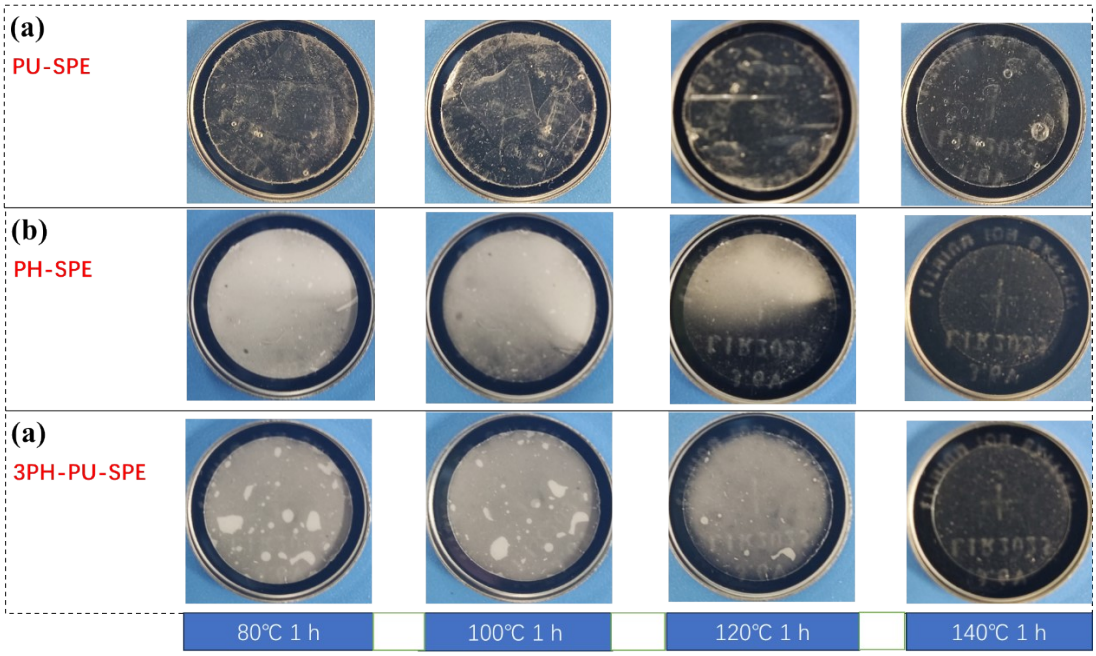

Fig. S5. Digital images of the (a) PU-SPE, (b)PH-SPE and (c) 3PH-PU-SPE films after heat exposure at different temperatures for 1 h.

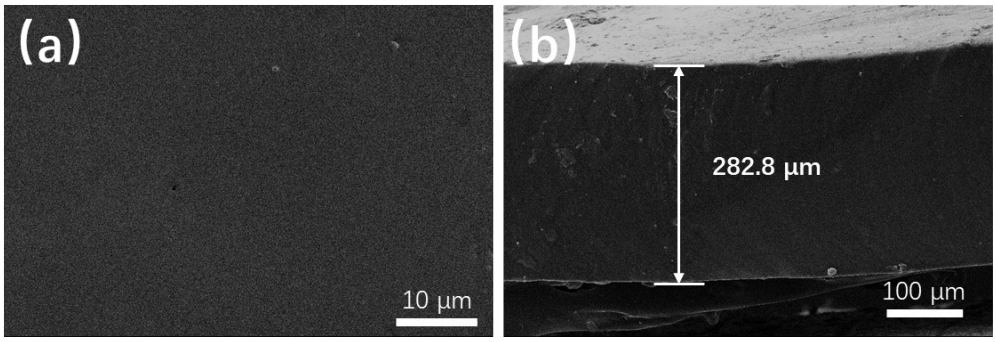

Fig. S6. SEM images of PU-SPE. (a) Top and (b) cross-sectional images.

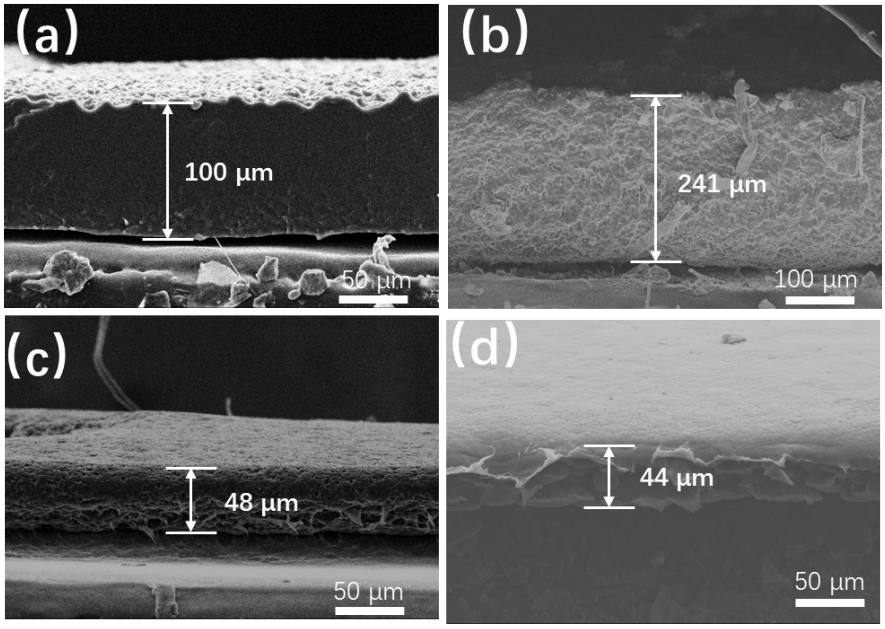

Fig. S7. SEM images of (a) PH-3PU-SPE, (b) PH-PU-SPE, (c) 3PH-PU-SPE and (d) PH-SPE.

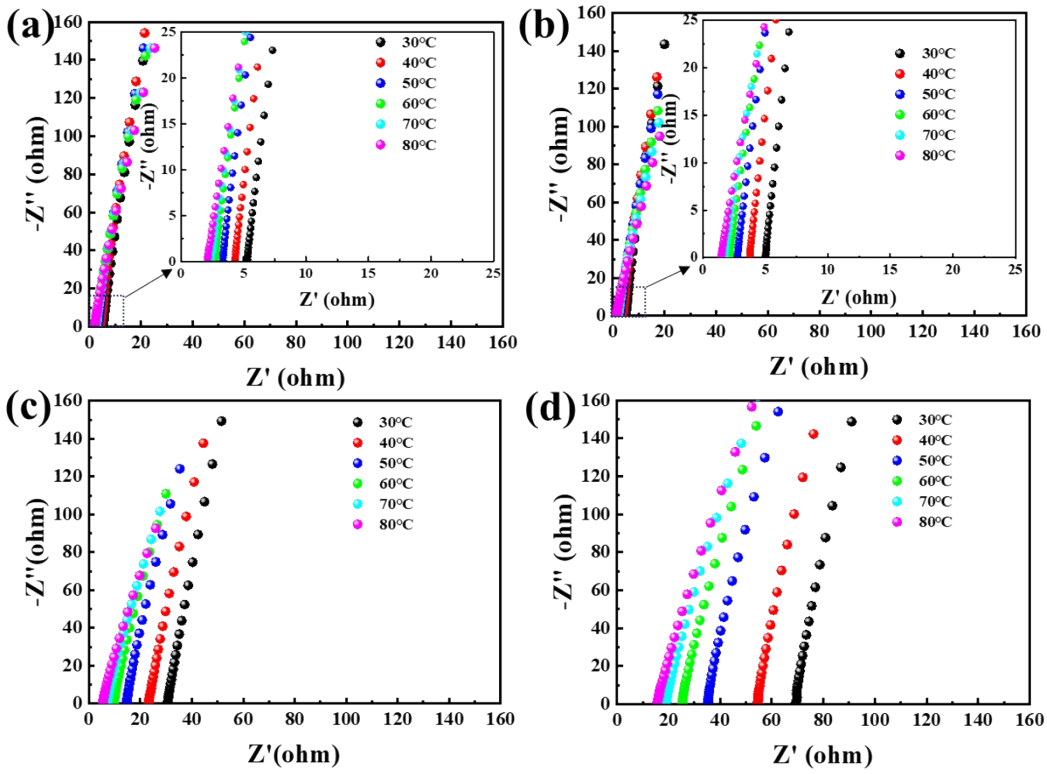

Fig. S8. Corresponding EIS plots of (a) PH-SPE, (b) 3PH-PU-SPE, (c) PH-PU-SPE and (d) PH-3PU-SPE at different temperatures.

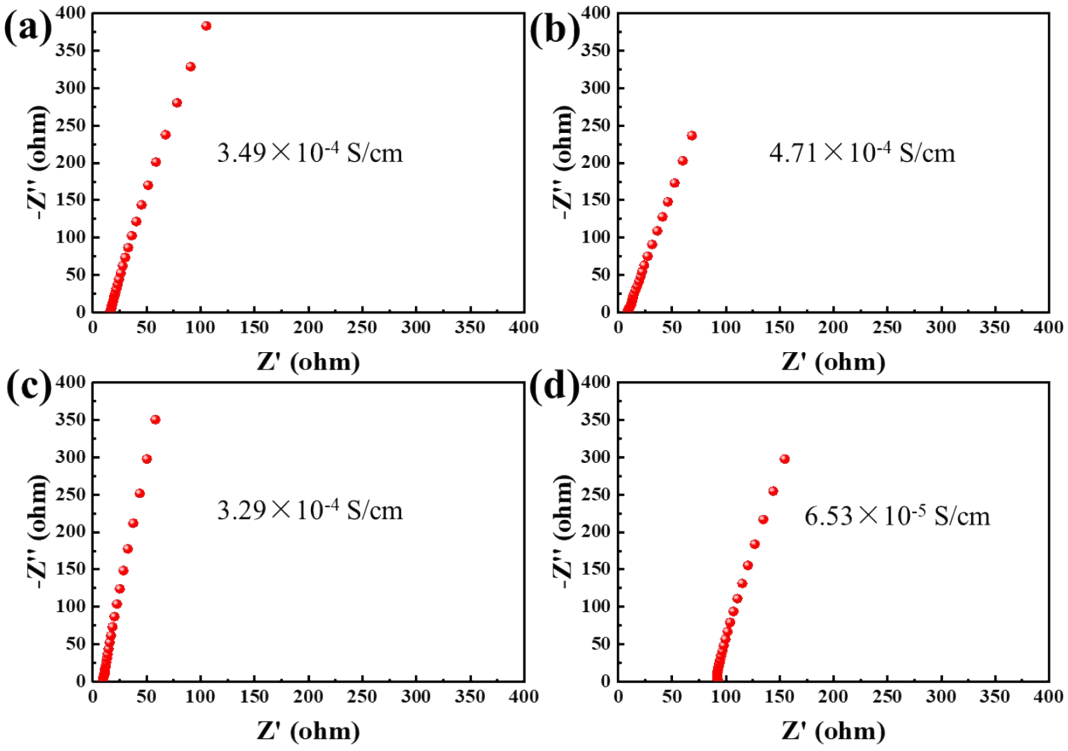

Fig. S9. Corresponding EIS plots of (a) PH-SPE, (b) 3PH-PU-SPE, (c) PH-PU-SPE, and (d) PH-3PU-SPE at room temperature.

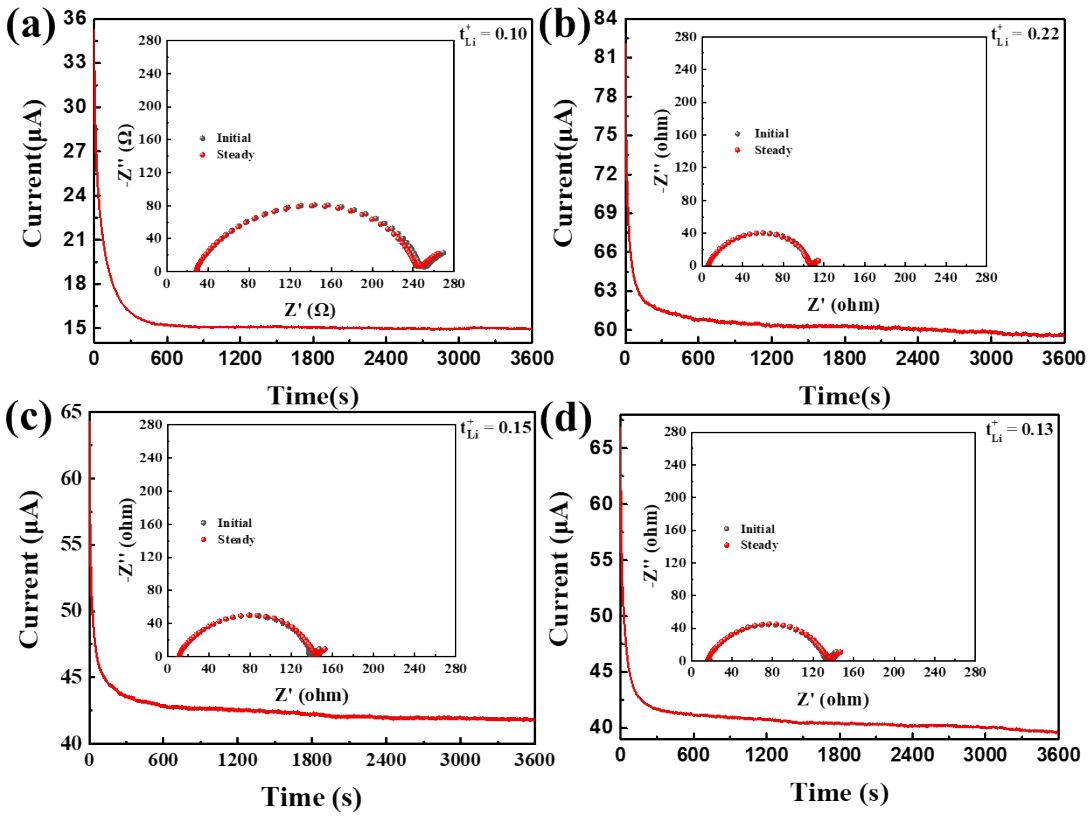

Fig. S10. *I-t* curves for Li symmetrical cells with (a) PH-SPE, (b) 3PH-PU-SPE, (c) PH-PU-SPE and (d) PH-3PU-SPE at a polarization voltage of 10 mV (insets are EIS plots before and after the polarization).

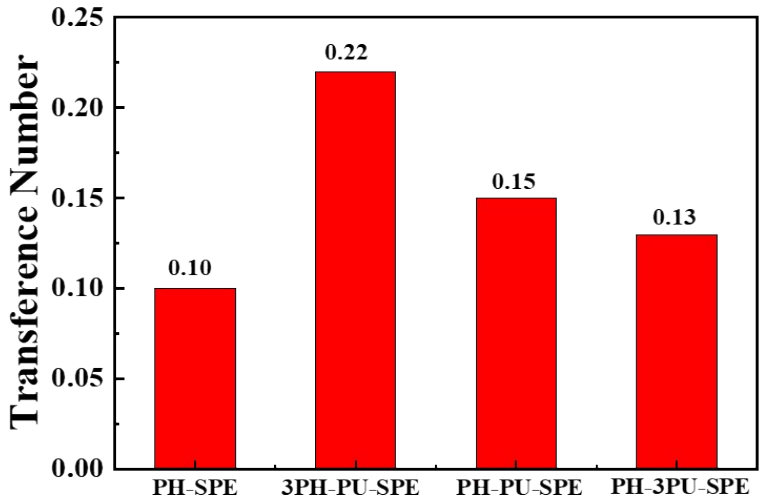

Fig. S11. Li^+ transference number of PH-SPE, 3PH-PU-SPE, PH-PU-SPE and PH-3PU-SPE.

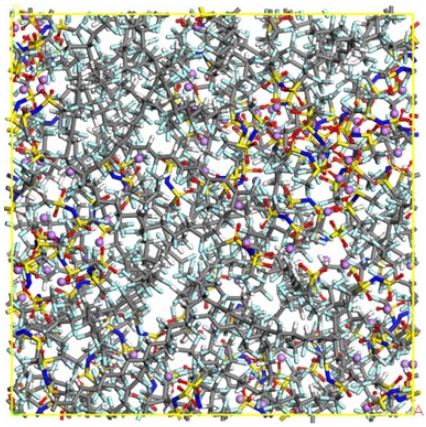

Fig. S12. Snapshot obtained from MD simulation on PH-SPE.

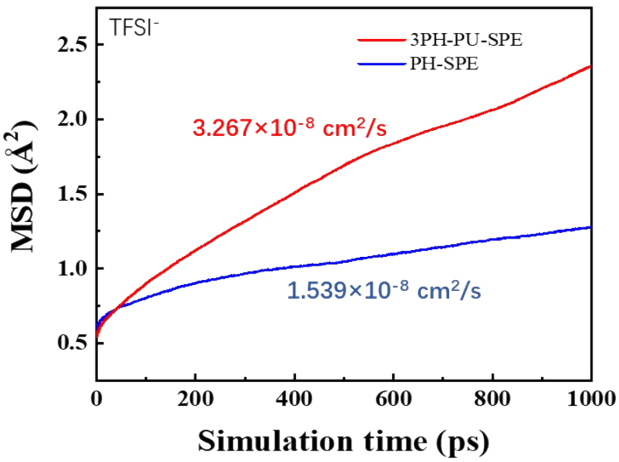

Fig. S13. Mean square displacement (MSD) of Li^+ in PH-SPE and 3PH-PU-SPE.

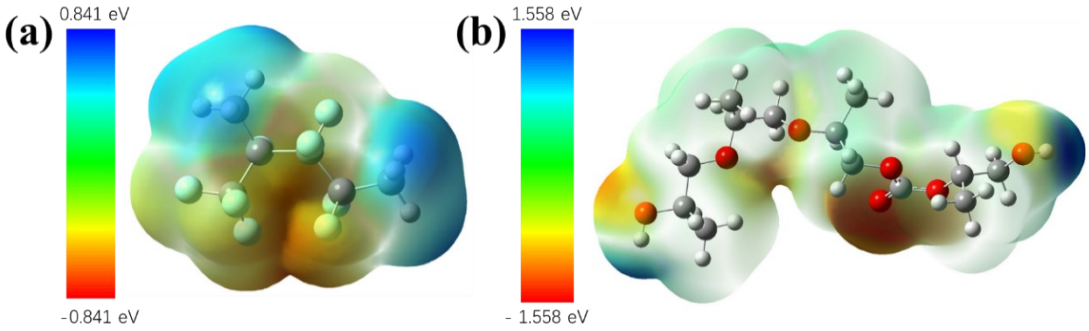

Fig. S14. Electrostatic potential distribution of (a) PVDF-HFP and (b) PPCD.

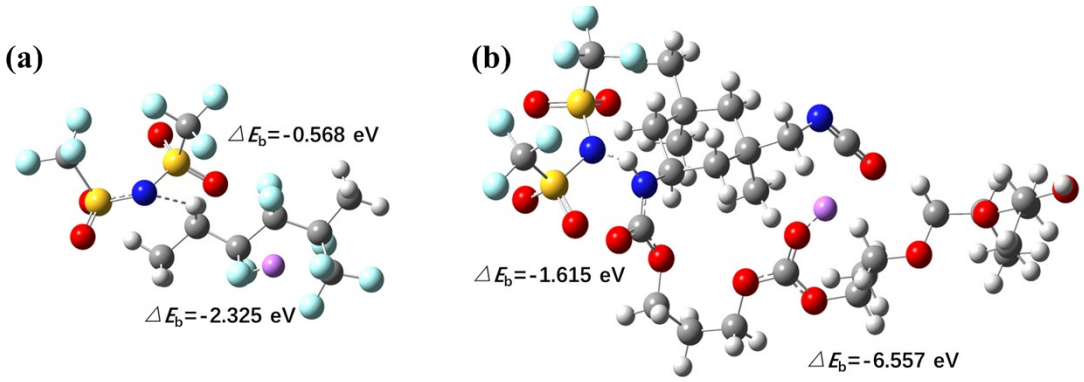

Fig. S15. Binding energies of Li^+ and $TFSI^-$ to (a) PVDF-HFP and (b) PU.

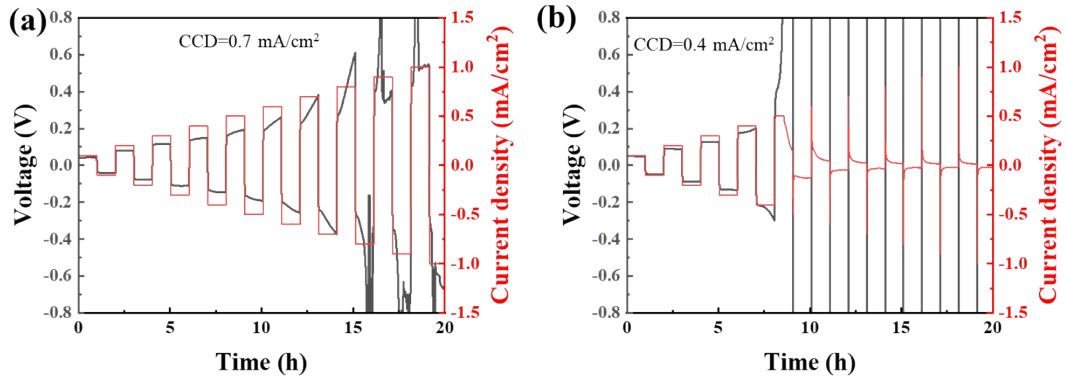

Fig. S16. Critical current density tests of symmetric (a) Li|3PH-PU-SPE|Li and (b) Li|PH-SPE|Li cells.

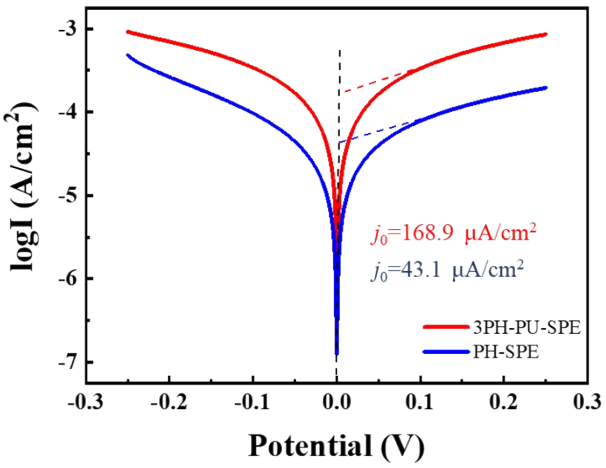

Fig. S17. Tafel plots of the Li||Li symmetric cells with the 3PH-PU-SPE and PH-SPE.

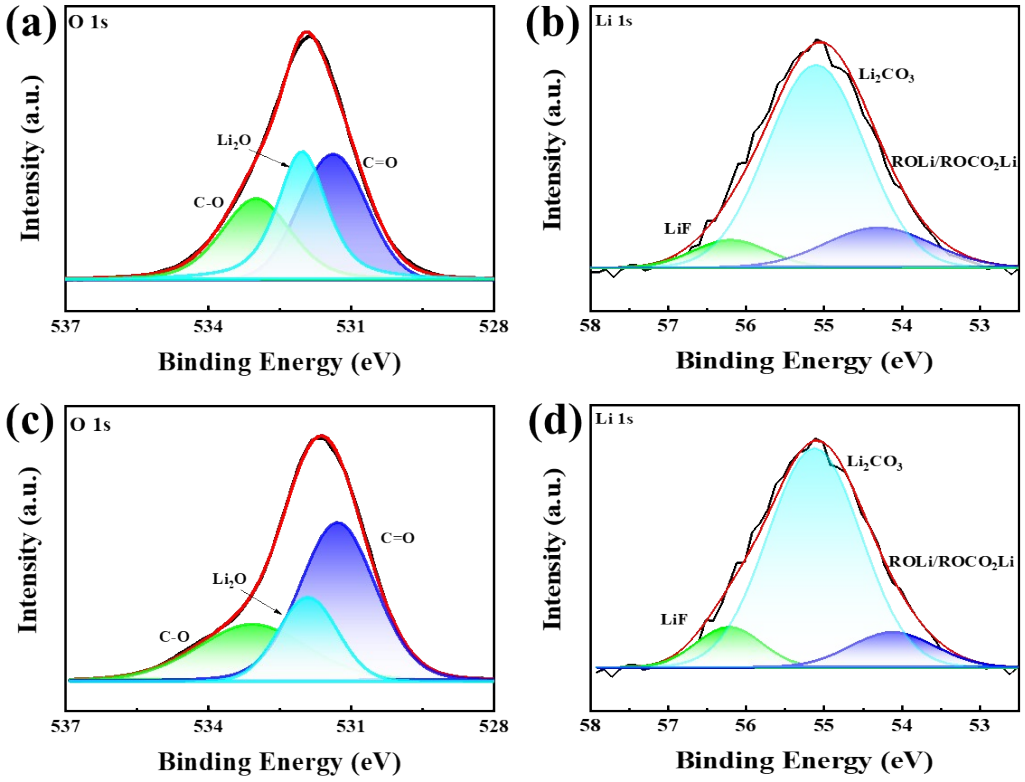

Fig. S18. (a) O 1s and (b) Li 1s spectra for Li anode of the symmetric Li|PH-SPE|Li cell. (c) O 1s and (d) Li 1s spectra for Li anode of the symmetric Li|3PH-PU-SPE|Li cell.

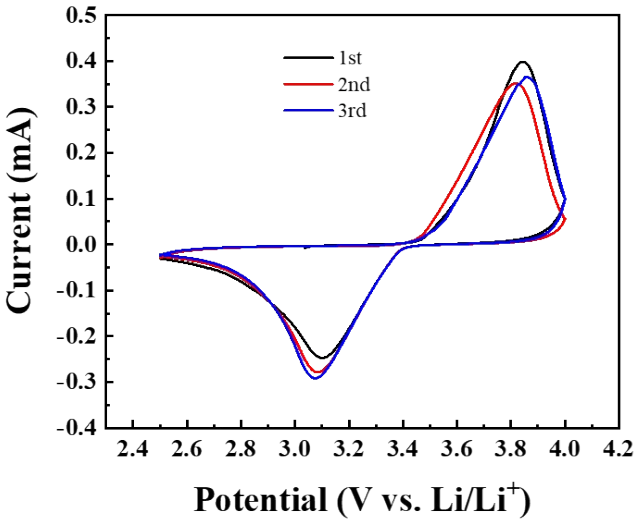

Fig. S19. Cyclic voltammetry curves of the solid-state Li|PH-SPE|LFP battery for the first three cycles at a scan rate of 0.1 mV/s.

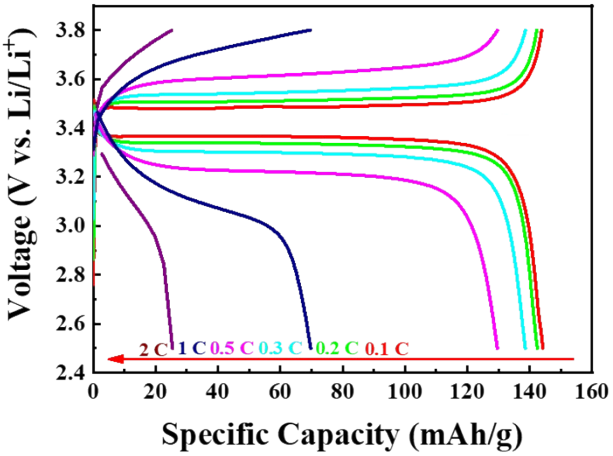

Fig. S20. Charging and discharging curves of the solid-state Li|PH-SPE|LFP battery at different rates.

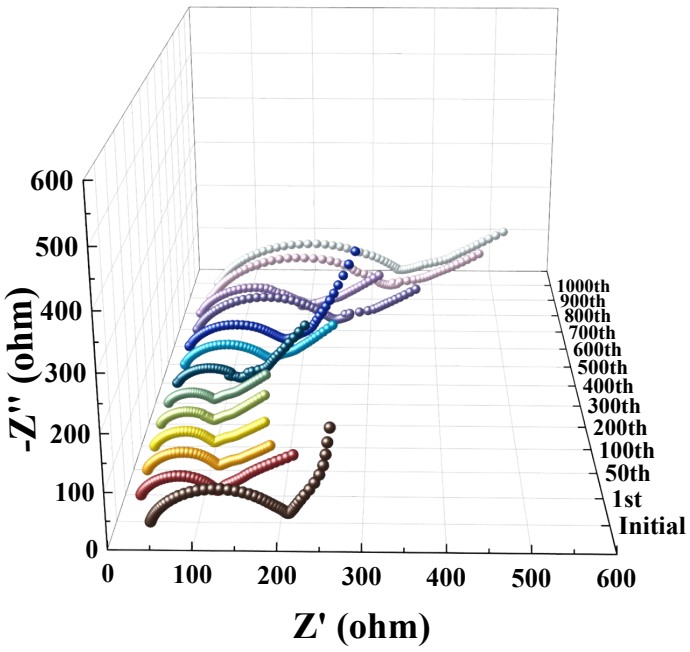

Fig. S21. EIS plots of the solid-state Li|3PH-PU-SPE|LFP battery before cycle and at different cycles at 0.5 C.

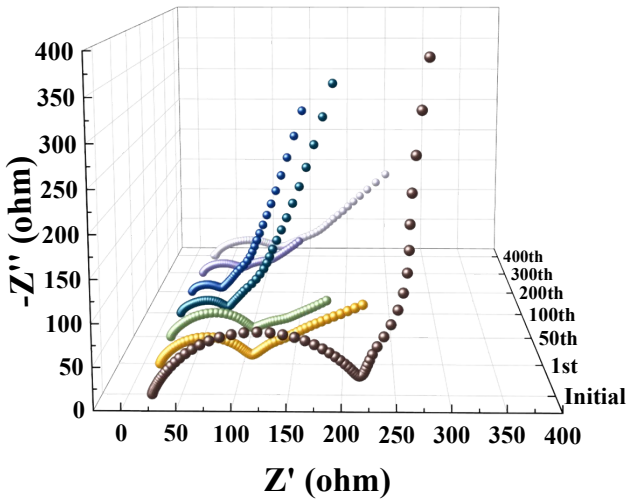

Fig. S22. EIS plots of the solid-state Li|3PH-PU-SPE|LFP battery before cycle and at different cycles at 1 C.

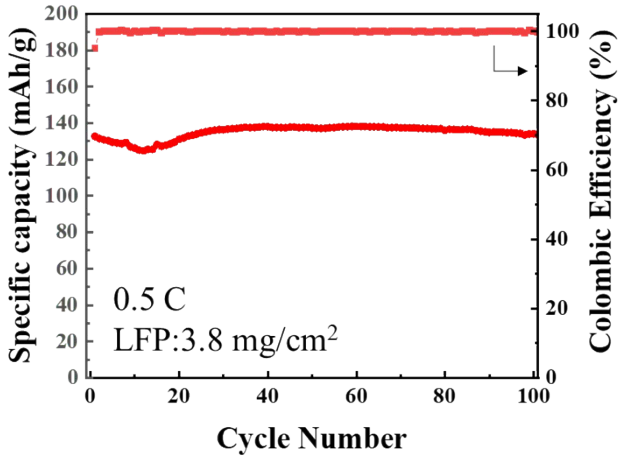

Fig. S23. Cycling performance of the solid-state Li|3PH-PU-SPE|LFP battery with a 3.8 mg/cm^2 LFP cathode at 0.5 C.

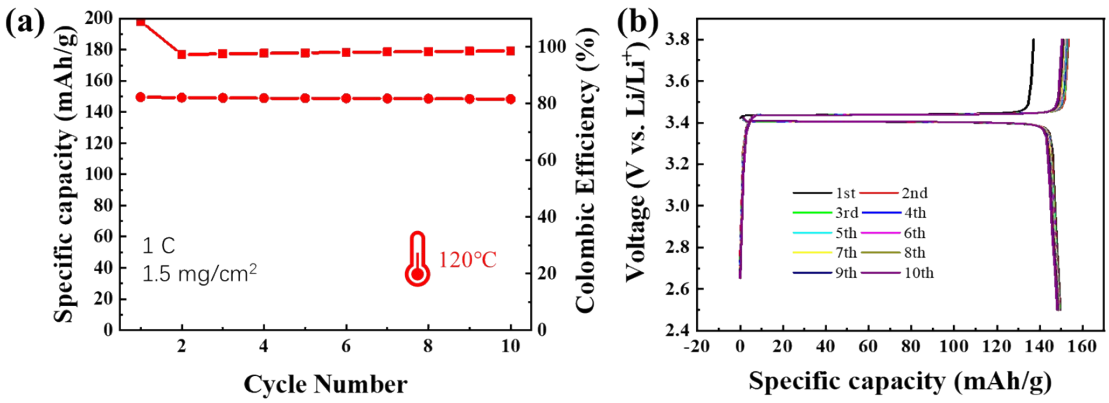

Fig. S24. (a) Cycling performance of the solid-state Li|3PH-PU-SPE|LFP battery at 120℃ and 1 C. (b) Charging and discharging curves of the solid-state Li|3PH-PU-SPE|LFP battery at 120℃ and 1 C.

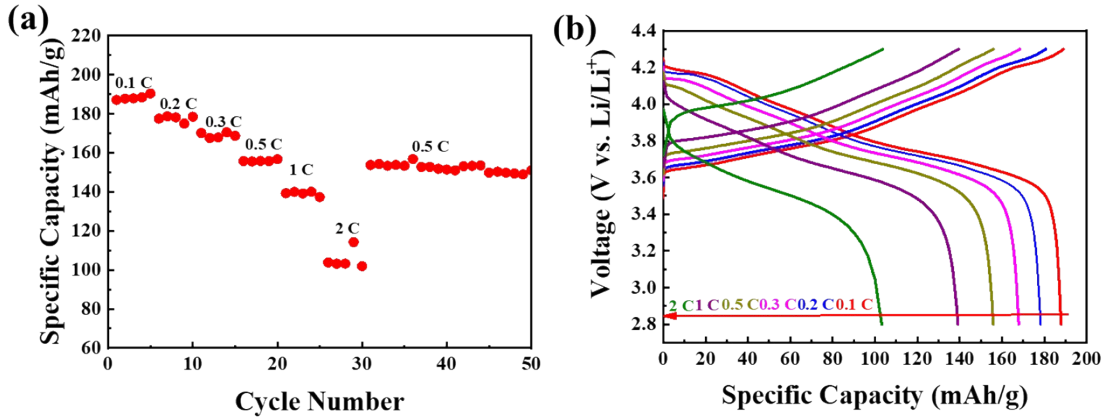

Fig. S25. (a) Rate capabilities of the solid-state Li|3PH-PU-SPE|NCM811 battery. (b) Charging and discharging curves of the solid-state Li|3PH-PU-SPE|NCM811 battery at different rates.

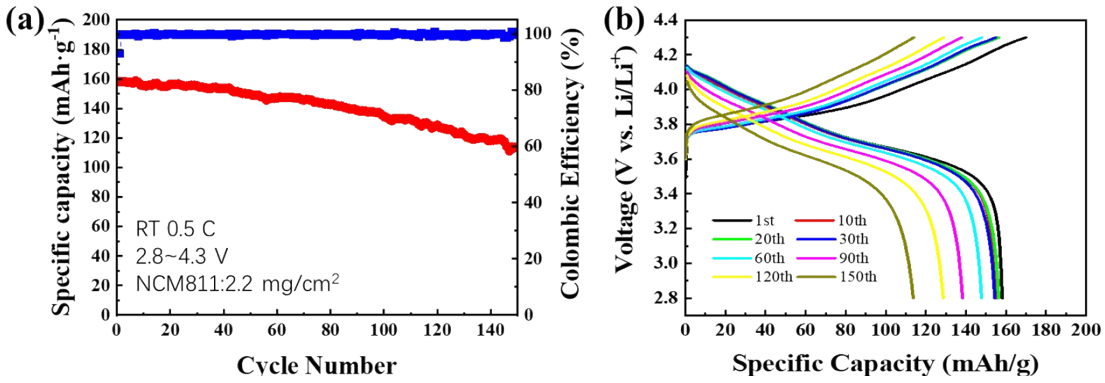

Fig. S26. (a) Cycling performance and (b) Charging and discharging curves of solid-state Li|3PH-PU-SPE|NCM811 batteries at 0.5 C.

Table S1. Comparison of the cycling performance for the solid-state Li||LFP batteries using different solid-state electrolytes.

Electrolyte	Battery	Temperature (°C)	Specific capacity (mAh/g)	Cycle number	Mass loading (mg/cm^2)	Rate	Reference
CNC-PVAc-PVDF-HFP-ZIF-8	Li||LFP	60	163.8	250	1.2	0.1 C	[1]
PEO-PVDF-HFP-CeO_2	Li||LFP	60	154.6	500	1.8-2.3	0.5 C	[2]
PEGDA-PVDF-HFP	Li||LFP	60	138.9	300	3	0.5 C	[3]
PVDF-HFP-PMMA-MOFs	Li||LFP	60	157.1	100	/	0.2 C	[4]
PVDF-HFP-$LiTa_2PO_8$	Li||LFP	55	165.8	100	~1.92	0.2 C	[5]
PVDF-HFP-PEO-$Li_7La_3Zr_2O_{12}$	Li||LFP	50	146.5	80	0.9	0.1 C	[6]
PVDF-HFP-PEGME	Li||LFP	80	155	100	1.5	0.5 C	[7]
PVDF-HFP-PU-SPE	Li||LFP	RT 90	138.1 150.1	1000 500	1.5-2.0	0.5 C 1 C	This work

References:

1. J. Mu, S. Liao, S. Wang, F. Xu, B. Su, L. Shi, X. Wang, X. Hao, Z. Guo, Z. Huang and T. Tian, *Advanced Functional Materials*, 2025, DOI: 10.1002/adfm.202519281.
2. T. Duan, J. Li, L. Li, Q. Sun, X. Lu and H. Cheng, *Energy Storage Materials*, 2024, **73**.
3. J. Ma, H. Jiang, L. Chen, Y. Wu, Y. Liu, W. Ping, X. Song and H. Xiang, *Journal of Power Sources*, 2022, **537**.
4. S. Wang, L. He, M. Wang, X. Guo, X. Qiu, S. Xu, P. Senin, T. Bian and T. Wei, *Particuology*, 2024, **93**, 203-210.
5. J.-M. Hong, J.-H. Kim, J. Sun, D.-H. Park, J.-S. Jang, G.-I. Lee, J.-W. Lim, S.-J. Park, M.-J. Kim, S.-Y. Jang, K. Min and K.-W. Park, *Materials Today Energy*, 2025, **49**.
6. G. Yu, Y. Wang, K. Li, S. Sun, S. Sun, J. Chen, L. Pan and Z. Sun, *Chemical Engineering Journal*, 2022, **430**.
7. Y. Shao, F. Alloin, D. Bresser and C. Iojoiu, *Journal of Materials Chemistry A*, 2024, **12**, 30032-30040.